

# The Soft-Confining Method for Creating Molecular Models of Amorphous Polymer Surfaces

Hongyi Liu,<sup>†,‡</sup> Yan Li,<sup>‡</sup> Wendy E. Krause,<sup>†</sup> Orlando J. Rojas,<sup>\*,†,§,||</sup> and Melissa A. Pasquinelli<sup>\*,†</sup>

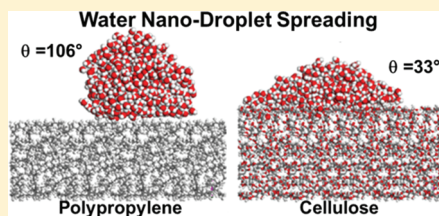
<sup>†</sup>Fiber and Polymer Science Program and the Department of Textile Engineering, Chemistry, and Science, North Carolina State University, Raleigh, NC 27695, United States

<sup>‡</sup>The KAUST-Cornell Center for Energy and Sustainability (KAUST-CU), Cornell University, Ithaca, New York 14853, United States

<sup>§</sup>Department of Forest Biomaterials, North Carolina State University, Raleigh, North Carolina 27695, United States

<sup>||</sup>Department of Forest Products Technology, School of Chemical Technology, Aalto University, P.O. Box 16300, FI-00076 Aalto, Finland

**ABSTRACT:** The goal of this work was to use molecular dynamics (MD) simulations to build amorphous surface layers of polypropylene (PP) and cellulose and to inspect their physical and interfacial properties. A new method to produce molecular models for these surfaces was developed, which involved the use of a “soft” confining layer comprised of a xenon crystal. This method compacts the polymers into a density distribution and a degree of molecular surface roughness that corresponds well to experimental values. In addition, calculated properties such as density, cohesive energy density, coefficient of thermal expansion, and the surface energy agree with experimental values and thus validate the use of soft confining layers. The method can be applied to polymers with a linear backbone such as PP as well as those whose backbones contain rings, such as cellulose. The developed PP and cellulose surfaces were characterized by their interactions with water. It was found that a water nanodroplet spreads on the amorphous cellulose surfaces, but there was no significant change in the dimension of the droplet on the PP surface; the resulting MD water contact angles on PP and amorphous cellulose surfaces were determined to be 106 and 33°, respectively.



## INTRODUCTION

By the 1980s, a great deal of research had been done on the physical structure and properties of polymeric materials.<sup>1</sup> A semicrystalline structure, defined as a mixture of crystal and amorphous domains, was proposed for most soft polymeric materials, especially textile synthetic fibers. The properties of polymeric systems differ depending not only on the molecular weight distribution but also on their geometry (e.g., fiber vs film) and the degree of molecular orientation and confinement. For example, the glass transition temperature ( $T_g$ ) in thin films decreases as the thickness decreases, thus providing evidence that interfaces play an important role.<sup>2</sup> Recent molecular dynamics (MD) simulations suggest that a similar surface effect for  $T_g$  depression can be expected for polymer fibers, which can impact their thermomechanical properties.<sup>3</sup> Since much experimental effort recently has been focused on developing uniform thin films of polymeric materials, an understanding of these effects is an important goal for optimizing the preferred characteristics.

Thin polymer films are desired for a variety of applications, including lab-on-a-chip devices,<sup>4</sup> biotechnology,<sup>5,6</sup> molecular detection,<sup>7,8</sup> and smart coatings.<sup>9</sup> Uniform polymer films can also be used as model experimental systems to investigate properties without the complications of structural and chemical heterogeneities that may exist in other geometries such as in a fiber.<sup>10</sup> Many techniques of thin film preparation are widely used for polymers, such as dip coating,<sup>11</sup> spin coating,<sup>12</sup> plasma coating,<sup>13</sup> chemical deposit coating,<sup>14,15</sup> and so on.<sup>16,17</sup> Thin, uniform films can be created by

actively spreading the coating material under centrifugal force in spin coating. Spin coating is done by first dissolving polymers in a volatile solvent, placing drops of the solution on a flat substrate, and then spinning the system into a uniform polymer film with a thickness ranging from a few nanometers to about a micrometer.<sup>18</sup>

Amorphous model cellulose films have been developed, and its molecular structure has been studied in many experimental efforts.<sup>19–25</sup> For example, it has been reported in recent experiments that ultrathin films of regenerated cellulose that had been immersed in water undergo changes in surface energy and supramolecular rearrangements.<sup>25</sup> In addition, thin films of polypropylene (PP) are desired for characteristics such as improved biocompatibility in its applications. Yan and Ren<sup>26</sup> spin-coated PP of varying tacticities and observed that isotactic PP was semicrystalline while atactic PP was amorphous; the amorphous film was also measured to be dramatically much smoother than the semicrystalline form. The structure and molecular weight of PP were observed to directly impact the thickness of the immobilized films.<sup>26</sup> The forces acting near the surface were determined through a systematic study to be dependent on the method of how the film was prepared.<sup>27</sup> In a recent study on surfactant interactions with thin films of PP, polyethylene, and cellulose, it was suggested that self-associated

**Received:** September 18, 2011

**Revised:** December 23, 2011

**Published:** January 31, 2012



and anchor-buoy-type structures were adsorbed from aqueous solutions, depending on the hydrophobicity as well as surface roughness of the substrate.<sup>28</sup> Our work also has highlighted how the nature of the solid surface impacts surfactant behaviors and assembly.<sup>29–31</sup> Because of the recent interest in studying the surface of thin films, there is motivation to build molecular models of amorphous polymeric layers and to investigate the physical properties at the atomic level. A polymer layer in a molecular model is a mimic of a thin film produced by spin-coating, for example, and therefore, compared to existing models used to predict bulk characteristics, it may capture more accurately the structural effects due to the presence of an interface.<sup>32–34</sup>

After the first atomistic modeling of amorphous glassy polymers done by Theodorou and Suter,<sup>35</sup> two different methods for producing amorphous polymer surfaces were developed and tested: a “free” polymer surface and a confined polymer surface.<sup>36</sup> The free polymer surface was created by arbitrarily elongating one of the box dimensions to a long coordinate and equilibrating the periodic system in isometric–isothermal (NVT) conditions, which were used by many others.<sup>37–43</sup> Unfortunately, this method can produce high and uncontrollable roughness, nonuniform density distributions, and a high surface energy that does not adequately represent the real system.

To create the confined polymer surface, a pair of dummy rigid surfaces was added in the confined dimension. The rigid surfaces could function as hard repulsive walls that arbitrarily rebound the atoms back into the MD box if the polymer atoms move close to it. This method works fairly well for polymers with a soft, single-chain backbone such as polyethylene, PP, polyvinylchloride (PVC), and polymethylmethacrylate (PMMA); however, challenges arise when applied to polymers with rings in their backbone, such as cellulose and polyethylene terephthalate (PET). In such cases, the rings fold unnaturally at the confined border due to the hard wall repulsions, which results in atomic clashes or higher potential energies. In addition, the confined polymer surface method can cause high density of the interface, as was observed for a PP film where the density at the surface was twice as high as that in the middle.<sup>36</sup> The free polymer surface method does not have this drawback, but the large and uncontrollable roughness can be a serious problem to study polymer surfaces, and also may not be the best representation of the real system.

The goal of this work is to build appropriate molecular models of thin films of both PP and cellulose. To overcome the limitations discussed previously of the free and confined surface methods, we apply a soft confined condition to build amorphous layers, which yields an appropriate level of molecular surface roughness. To validate these models, each layer was subjected to MD simulations to predict their physical properties and compared to experiments. In addition, the hydrophobicity of the PP layer and the hydrophilicity of the cellulose layer were investigated by calculating the contact angle (CA) of water nanodroplets on each surface and compared to experimental values, such as those for crystalline cellulose surfaces obtained by Mazeau and co-workers.<sup>50</sup>

## METHODOLOGY

All work was performed with the Materials Studio 4.1 software of Accelrys Inc.<sup>51</sup> Unless explicitly stated otherwise, all MD simulations were performed with a default time step of 1 fs and temperature of 298 K. All work was done on a Dell SC1420 workstation with Windows server 2003, dual Intel Xeon 2.8 GHz CPUs, and 4 GB of RAM.

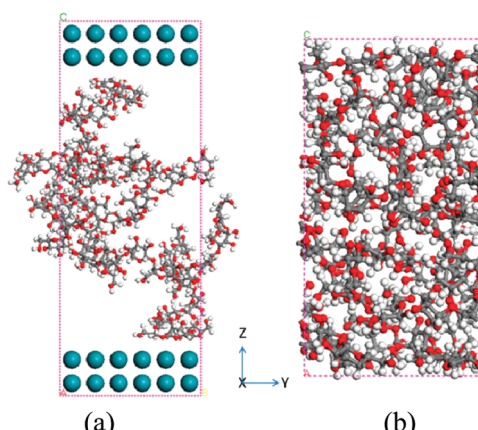


**Figure 1.** Preparation of the cellulose surface. (a) The xenon-cellulose-xenon cell before the MD equilibration procedure and (b) the cellulose unit layer created from (a). Results are qualitatively similar for PP. Red is oxygen; gray is carbon; white is hydrogen; blue is xenon.

**Construction of the Polymer Chains.** PP and cellulose are two of the most commonly used amorphous surfaces. In addition, cellulose molecules have 6-membered pyranose rings that are useful to verify the method proposed in this work. The structures of the cellulose and PP repeat units, i.e., 1,4- $\beta$ -D-glucopyranose and propylene, are provided by the library of Materials Studio 4.1 software. The atom properties are defined by the COMPASS force field.<sup>52</sup> The cellulose molecule is built with 8 repeat units (1,4- $\beta$ -D-glucose) a head-to-tail orientation, and isotactic tacticity. Thirty propylene repeat units are employed to construct the PP molecule under the same conditions. After a 5-ps minimization in vacuum, the end-to-end distances of cellulose and PP molecules are 42.5 and 76.7 Å, respectively.

**Creation of the Initial Unit Layers of the Confined Amorphous Polymer.** The minimized molecular structure of the polymer chains is used to build a unit layer for each substrate; the “unit” indicates that the system can be easily expanded to a larger layer. The polymer molecules can be packed into a confined layer or a periodic cell with Amorphous Cell.<sup>51</sup> We selected the confined layer to build the thin substrate of polymers, such that polymer interactions in the  $xy$  plane are enabled, but their movement in the  $z$  direction (the direction perpendicular to the surface) is restricted. Figure 1a illustrates this setup. An ideal confining surface is a solid at the desired temperature, ultraflat and uniform (square faceted is ideal), and has little or no attractive interactions with the polymer atoms. Although no such atomic system exists in reality, a xenon crystal is selected as the confining layer since it has a flat crystal slice, inert character, and is solid at 298 K. The COMPASS force field is used with the 9.5-Å group-based cutoff. Specific adjustments for each polymer type are given in the next two sections.

**Creation of the PP Confined Unit Layer.** Three PP molecules are first built in the confined layer directly by Amorphous Cell with a referenced value of 0.822 g/cm<sup>3</sup> as the initial density. The lengths of the  $x$  and  $y$  dimensions of the surface are set to 16.7 Å, which is identical to those of the reference xenon crystal. Using the “Fix Fractional Position” option, the PP unit layer is inserted between two xenon crystal substrates. The fractional  $xyz$  position property in the fractional space of the lattice is kept constant for the selected xenon atoms, which means that the motion of the xenon atoms is constrained. In general, PP is too

soft to be compacted since it lacks a ring, bulky side group, or unsaturation along the backbone, and thus isometric conditions are necessary. A 50-Å-thick vacuum space is added to the top of the box to diminish the periodic interruption along the  $z$  axis. After performing NVT equilibration for 50 ps and dynamics for 1 ns, the vacuum space and two xenon crystals are cropped off by using the cell building feature. The dimension of the resulting surface is  $16.7 \times 16.7 \times 26.0 \text{ \AA}^3$ .

**Creation of the Cellulose Confined Unit Layer.** Since cellulose contains rings along its backbone, its chain can be compacted, and thus isobaric conditions are needed initially to create the surface. Six cellulose molecules are first built in the confined layer directly by Amorphous Cell; a low-enough initial density of  $0.5 \text{ g/cm}^3$  is arbitrarily chosen, and the initial lengths of the  $x$  and  $y$  dimensions of the surface are set to 23.6 Å. Just as with PP, the “Fix Fractional Position” option is used to insert the cellulose unit layer between two xenon crystal substrates, and the xenon atom positions are held constant. The vacuum space is not necessary for cellulose because its volume is variable under the isobaric condition. NPT dynamics are first performed to adjust the density of the system, and then NVT dynamics are used to further equilibrate the system. The NPT dynamics are performed with a pressure of 100 kPa (approximately equal to 1 atm) and include an equilibration for 100 ps followed by 1 ns of dynamics. Then 500 ps of NVT dynamics is run. The resulting structure is depicted in Figure 1b. Additional parameters are the same as the method used for PP, including the removal of the confining layers. The dimension of the resulting surface is  $16.7 \times 16.7 \times 31.5 \text{ \AA}^3$ .

**Construction of Super Layers.** Because of the periodic border in the  $xy$  plane, the layer is expanded to a super layer in the  $x$  and  $y$  directions. The super layer is composed with  $x$  and  $y$  lattice vectors which are integral multiples of their equivalents in the original unit. The  $z$  direction is confined and not expandable. For analysis of all other properties but the CA, the expansion multiple is set to 2 in the  $x$  and  $y$  direction and kept to 1 in the  $z$  direction. Therefore, each super layer is created to have a surface area four times larger than the original “unit” layers; the resulting structure for cellulose is given in Figure 1b. The total size of the super layer is given in Table 1. Larger surfaces are required for creating CA models due to the size of the water nanodroplet; therefore, the expansion multiple is set to 4 in the  $x$  and  $y$  direction, and kept to 1 in the  $z$  direction, which led to super layers whose surface areas are  $4 \times 4$  times that of the unit layers.

**Construction of Bulk Models.** The bulk models with 3-D periodic boundary conditions are built with the same number of molecules and the dimension with the corresponding film models. Then 500 ps of NPT dynamics with a pressure of 100 kPa and a temperature of 298 K is performed with each bulk model to obtain an appropriate bulk density under room conditions. Then another 500 ps of NVT dynamics is carried out to reach thermal dynamic equilibrium. For the calculation of the bulk properties, 40 frames of the last 200 ps are used.

**Calculation of Surface Properties.** The cohesive energy density (CED) is calculated with the analysis function of Materials Studio 4.1. The expanded layers of PP and cellulose are used in the CED analyses. The thermal volumetric expansion is calculated by using the stepwise temperature procedure as implemented by the Temperature Cycle protocol in Amorphous Cell. The procedure performs a stepwise, constant-pressure MD heating and/or cooling process; the pressure is set to 100 kPa, the lower and upper temperatures are fixed at 200 and 800 K, respectively, and 5 temperature stages are used for 500 ps each with 298 K as the starting temperature. In addition, 200 ps are set as

**Table 1. Calculated Properties of the Confined Layers of PP and Cellulose from the MD Simulations and Values from the Literature for Comparison<sup>a</sup>**

	PP	cellulose
unit layer dimensions ( $\text{\AA}^3$ )	$33.3 \times 33.3 \times 26.0$	$33.3 \times 33.3 \times 32.3$
surface area ( $\text{\AA}^2$ )	1366	1384
surface roughness	1.23	1.25
density ( $\text{g/cm}^3$ )	0.87	1.45
exptl (amorphous)	$0.86^{57}$	---
exptl (crystalline)	$0.95^{57}$	$1.60^{55}$
other simulations	$\sim 0.75^{43}$	$1.38-1.42^{60,61}$
CED ( $10^8 \text{ J/m}^3$ )	$2.1 \pm 0.1$	$4.9 \pm 0.1$
electrostatics and H-bonding	(negligible)	$4.5 \pm 0.1$
van der Waals	$2.1 \pm 0.1$	$0.4 \pm 0.1$
solubility parameter	$14.5 \pm 0.1$	$22.2 \pm 0.2$
$(\text{J/cm}^3)^{0.5}$		
electrostatics and H-bonding	$0.4 \pm 0.1$	$21.1 \pm 0.1$
van der Waals	$14.5 \pm 0.1$	$6.6 \pm 0.5$
exptl work	$16.2-19.3^{56,62}$	$23.5-28.0^{63}$
other simulations	$16.1^{53}$	$34.8^{53}$
Gibbs surface energy <sup>64</sup>	$62.7 \pm 14.4$	$81.7 \pm 20.5$
$(\text{mJ/m}^2)$		
nonbond surface energy	$26.7 \pm 6.4$	$68.1 \pm 17.0$
van der Waals	$24.1 \pm 6.6$	$82.4 \pm 16.8$
electrostatics	$2.6 \pm 0.7$	$473.0 \pm 125.2$
H-bonding	N/A	$-487.2 \pm 111.5$
number of H-bonds	N/A	$5.6 \pm 1.3$
$(10^{-6} \text{ mol/m}^2)$		
valence surface energy	$36.0 \pm 8.2$	$13.6 \pm 4.1$
exptl	$27.6-34.8^{65}$	$70.5^{66}$
second-order phase transitions (K)	361	$383, 525-571$
$T_g$ experimental work	$253-273^{67}$	$>513^{33}$
$T_g$ other simulations	$335-365^{43}$	$243-650^{61}$
thermal expansion ( $10^{-4} \text{ K}^{-1}$ )	$4.2 (<361 \text{ K})$	$1.5 (<383 \text{ K})$
	$11.0 (>361 \text{ K})$	$2.2 (>383 \text{ K})$

<sup>a</sup>The solubility parameters from the experiments are for bulk polymers, and for the other simulations, they are calculated from the topology method.

the average period of one cycle, and one-half-cycle is executed in total. Other dynamics parameters are the default values as above.

**Calculation of the Water–Surface Interaction Energy.** A layer-by-layer model is built to calculate the water–surface interaction. The water layer is constructed using Amorphous Cell with 1500 water molecules at the density of  $1 \text{ g/cm}^3$  and a temperature of 298 K, and the dimension of the water layer is  $33.3 \times 33.3 \times 40.4 \text{ \AA}^3$ . In the layer-by-layer model, the corresponding polymer layer (PP or cellulose) is at the bottom, the water layer is in the middle, and a 100-Å-thick vacuum space is set on the top so that only one surface of the polymer layer is affected by the periodic boundary conditions. NVT dynamics is carried out for 1 ns while the polymer layer is frozen. Of the last 500 ps, 100 frames are exported for further analysis. The interaction energies and hydrogen bonds between the polymer and water layers are calculated by a Perl program modified from our previous work.<sup>53</sup>

**Construction of CA Models.** First, a water nanodroplet is created. Initially, 500 water molecules are built into a periodic cube with a density at  $1.0 \text{ g/cm}^3$  using Amorphous Cell.

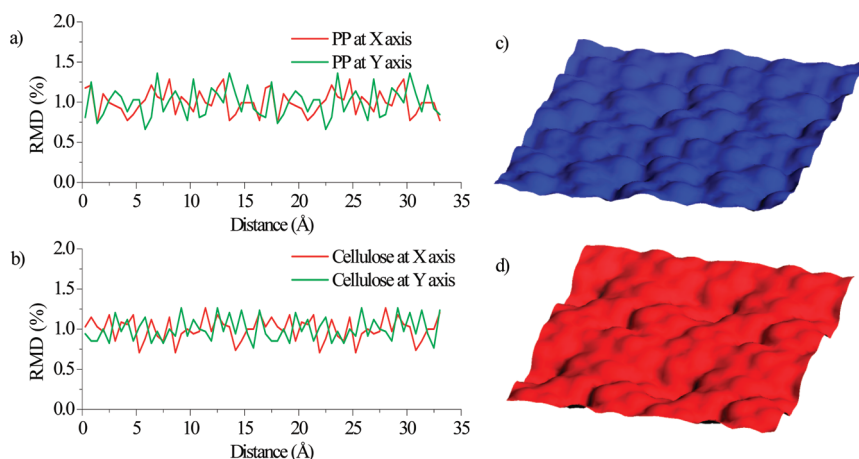


**Figure 2.** The relative mass distribution (RMD) of the confined amorphous layers of (a) PP and (b) cellulose along the  $x$  and  $y$  directions. The corresponding surface image is also depicted for (c) PP and (d) cellulose, both with dimensions of  $33.3 \times 33.3 \text{ Å}^2$ .

The cubic lattice is then removed to cancel the periodic conditions at the boundaries. Then, 500 ps of NVT dynamics without periodic boundary conditions are performed and the water cube becomes a water sphere, or nanodroplet, with a diameter of approximately 32 Å. The CA models are built by adding a 100-Å-thick vacuum space on the larger super layers, followed by placing the water nanodroplet on the confined super layers. The center of the water nanodroplet is centered at 16 Å above the surface. MD simulations with NVT dynamics time are run for 1 ns with both surfaces.

## RESULTS AND DISCUSSION

Molecular models of amorphous thin films of cellulose and PP were created by using a soft wall boundary and then equilibrated via MD simulations. The physical properties of these simulated thin films were characterized and compared to known experimental quantities, which will be described next.

**Calculation of Surface Properties.** The weight distributions along the  $x$  and  $y$  dimensions of the confined amorphous films of both the PP and cellulose are given in Figure 2, which are generated by dividing the surface into 100 slices in each direction and determining the number of atoms by the weight percentage in each slice. In addition, the surface area of each thin film calculated with the method described by Düren and co-workers<sup>54</sup> is indicated in the figure. Parts a and b of Figure 2 indicate that the relative mass distributions of both the PP and cellulose layers are slightly oscillating but still quite stable within 1% in the  $x$  and  $y$  directions, and the surface is relatively smooth (parts c and d of Figure 2). Therefore, both the PP and cellulose thin films can be considered sufficiently uniform in the  $xy$  plane. The surface areas for the images in parts c and d of Figure 2 are 1366 and 1384 Å<sup>2</sup> for PP and cellulose, respectively. The resulting roughness ratios (the surface areas per unit packing area) are 1.23 and 1.25 for PP and cellulose, respectively (Table 1). The uniformity and smoothness of the amorphous layers highlight the advantage of using the xenon crystal to confine the layer during the surface formation in the MD simulations.

Other properties that were calculated from the MD simulations are given in Table 1, along with values from the literature for comparison. The table indicates that for the thin film of cellulose, its density was calculated to be 1.45 g/cm<sup>3</sup>, which is approximately 10% lower than the experimental value for crystalline cellulose.<sup>55</sup> Since amorphous densities generally tend to be

10–20% lower than that of the crystalline phase, the calculated density for the cellulose thin film lies slightly above what would be expected for amorphous cellulose. In addition, the density of the molecular model of the cellulose thin film is slightly higher than those calculated from a periodic cell,<sup>56</sup> as expected since confinement can lead to a higher density. For the thin film of PP, the density of 0.87 g/cm<sup>3</sup> is slightly above the experimental value for amorphous PP and below the value for crystalline PP.<sup>57</sup> Therefore, the density values, weight percentage distributions, and surface areas for both thin films built with the soft confined condition are within typical ranges for these systems, thus both molecular models are reasonable representations of thin films of PP and cellulose.

The CED quantifies the intermolecular interactions among the polymer chains. The value of the CED for cellulose in Table 1 is twice that of PP, indicating a stronger intermolecular force in a specified volume, which is due to the intra- and inter- hydrogen bonds that are formed within cellulose chains. The contributions to the CED values from electrostatics and van der Waals interactions are also given in Table 1. The electrostatic forces are negligible for PP but are the strongest contribution for cellulose; for cellulose, the van der Waals interaction is nearly one-tenth of the electrostatic interaction. These contributions also point toward the significance of electrostatic intermolecular interactions (including hydrogen bonding) in cellulose systems that are confined in one dimension.

CED is a fundamental property of a polymer and many other properties can be predicted from it. For example, the solubility parameter ( $\delta$ ) can be calculated from the simple relation  $\delta = (\text{CED})^{1/2}$ . The solubility parameter quantifies the solvent–solute interactions that may be strong enough to separate solvent–solvent and solute–solute molecules as a means of minimizing the Gibbs free energy of the entire system. The values in Table 1 indicate that the solubility parameters derived from the molecular models of the thin films are lower than those of bulk polymers, whether obtained from experiments<sup>62,56,63</sup> or simulations (using the same force field).<sup>53</sup> The reason for the difference might be caused by three factors. The first is related to the confined condition, whereby the materials of the confined layer are not continuous in the confined direction, causing the CED of the confined layer to be lower than the bulk material, and thus a lower solubility parameter is obtained. Second, PP and cellulose are

typically semicrystalline, and only molecular models of amorphous layers were built and investigated in this report. Finally, because of the size limitations in the present MD simulations, the amorphous layers were built from much smaller molecular weight chains (oligomers) than is typical in real materials. Since oligomers have higher conformational freedom than macromolecules, the solubility parameter of oligomers is lower than that of polymers. The same is true for surface atoms, as compared to bulk.

The surface energy ( $\gamma$ ) is one of the most important properties for characterizing a surface, which is related to the disruption in intermolecular interactions when new interfaces are created. For free surfaces, the surface energy can be calculated as the excess energy at the surface of a material compared to the bulk, i.e. the Gibbs definition,<sup>64</sup> which is adapted to the case of polymer films according to the following equation,

$$\gamma_{\text{Gibbs}} = \frac{E_{\text{film}} - E_{\text{bulk}}}{2A} \quad (1)$$

where  $E_{\text{film}}$  and  $E_{\text{bulk}}$  are the potential energy of a polymer film and a bulk system of the same size, respectively, and  $A$  is the surface area (from Table 1). The factor of "2" in the denominator is due to the two exposed surfaces of the film.

The Gibbs surface energy and individual contributions of this surface energy are given in Table 1. The Gibbs surface energies of both the PP and cellulose confined layers are higher than the experimental values of the corresponding free surfaces (note that the value given for cellulose is for a semicrystalline free surface). However, the nonbond surface energies of both PP and cellulose are in agreement with the experimental values. For the individual nonbond contribution of PP, both the van der Waals and the electrostatic energies are positive, with the latter being the dominating factor.

For cellulose, the electrostatic surface energy is positive, while the H-bond energy is negative. Both absolute values of these energies are much higher than the van der Waals contribution. There are  $5.6 \pm 1.3 (10^{-6} \text{ mol/m}^2)$  hydrogen bonds that are broken for the construction of one amorphous cellulose surface. The electrostatic and the H-bond energies balance to a small negative number, while the van der Waals component is a comparable large positive component of the nonbond surface energy. The cellulose surface energy and its components have significantly larger standard deviations than those of the PP layer, which is due to the hydrogen bonds in amorphous cellulose having the freedom to break and reform with molecular thermal movements.

Therefore, different from the free surface, a confined surface model is employed in this work, not only to keep a suitable roughness but also a reasonable value for the surface energy. For the confined surface, confinement leads to the excess energy more than that of the free surface, due to bending or/and compressing the polymer molecules into a plane. To eliminate the extra excess energy, all atom positions in the confined layer (surface) are constrained, so that the covalent components are ignored and only nonbond interactions are effective in the surface energy.

The volumetric thermal expansion values of the molecular models of thin films of amorphous PP and cellulose were obtained from the stepwise temperature procedure; we defined the upper temperature to be 800 K, which is much higher than the thermal decomposition temperature of the polymers. Thermal decompositions involve breaking covalent bonds, which is beyond the capability of classical MD simulations and thus is not expected to occur during these simulations. Therefore, the higher

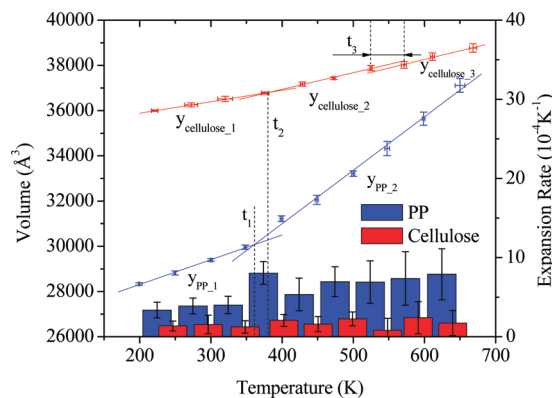


**Figure 3.** Volumetric thermal expansion of amorphous layers of PP (blue) and cellulose (red) are shown to the left  $y$  axis, with both  $x$  and  $y$  error bars. The thermal expansion of each pair of adjacent states is shown to the right  $y$  axis, PP with blue columns and cellulose with red columns. The volume data were grouped by sharp increase or decrease of the thermal expansions and the lowest standard error. The values for the fitting lines are given in Table 2. The  $t_1$  and  $t_2$  quantities are the cross points of these fitting lines at 361 and 383 K, respectively;  $t_3$  is the temperature range, 525–571 K.

**Table 2. The Slope and Intercepts for the Fitting Lines from Figure 3**

$y$ value	slope	intercept
$y_{\text{PP},1}$	11.0	26118.0
$y_{\text{PP},2}$	23.6	21538.2
$y_{\text{cellulose},1}$	5.1	34880.9
$y_{\text{cellulose},2}$	7.3	34004.6
$y_{\text{cellulose},3}$	7.7	33678.0

temperature values are utilized for comparison purposes, as such ranges can be considered as an example of the system at the limit of excess energy. In general, a linear relationship is expected between the volume and the temperature for these thin polymer films, so any deviations from this linearity can be taken as an indication of a change in the order within a system. An abrupt discontinuity indicates a first-order phase transition, such as melting or vaporization, whereas a subtle change is indicative of some form of a second-order phase transition, such as the glass transition temperature ( $T_g$ ) or a significant change in a hydrogen bonding network.

For the PP layer in Figure 3, the volumetric thermal expansion is composed of two linear regions with different slopes, indicating a second-order phase transition at the intersection of those lines, which is at 361 K. This value is within the range of the  $T_g$  values calculated from other simulations<sup>43</sup> but is significantly higher than the experimental values.<sup>67</sup> In general, the  $T_g$  for this system is expected to be below the experimentally observed ones for two reasons. One, shorter chains than commonly exist in experiments were used in the simulations, which tends to lower  $T_g$ . In addition, confinement due to the thin film structure is expected to lower the  $T_g$  by 30–70 K. Recent MD simulations on atactic PP systems suggested that this  $T_g$  depression could be due to both an increase of free volume and inhibition of the kinetic energy through higher barriers for conformational transitions of the backbone polymer atoms and "coupling rotations."<sup>43</sup> Thus, the observed second-order phase

**Table 3. Calculated Properties of the Confined Layers of PP and Cellulose Interacting with Water and Values from the Literature for Comparison**

	PP	cellulose
interaction energy ( $\text{mJ/m}^2$ )	$-41.0 \pm 2.5$	$-179.5 \pm 8.6$
van der Waals ( $\text{mJ/m}^2$ )	$-40.0 \pm 2.4$	$-47.3 \pm 5.7$
electrostatic ( $\text{mJ/m}^2$ )	$-1.0 \pm 0.4$	$100.7 \pm 17.9$
H-bond ( $\text{mJ/m}^2$ )	N/A	$-232.9 \pm 22.1$
no. H-bonds ( $10^{-6} \text{ mol/m}^2$ )	N/A	$11.1 \pm 1.1$
peak of relative density of water ( $d = \rho/\rho_0$ )	1.18	1.38
distance of water layer from surface ( $h, \text{\AA}$ )	2.11	2.23
CA of water nanodroplet (deg)	$106 \pm 4$	$33 \pm 3$
exptl	103–108	$23.8 - 49.7^{21,65}$
other simulations	$102^{49}$	$70 - 120^{50}$ (crystalline)

transition at 361 K is likely not due to  $T_g$ ; the  $T_g$  for this molecular model is expected to be below 200 K. The melting point of PP is around 400 K and thus could be a source of this observed transition. The coefficient of thermal expansion can be calculated from the slope of the lines, yielding a value of  $4.2 \times 10^{-4} \text{ K}^{-1}$  below 361 K and  $11.0 \times 10^{-4} \text{ K}^{-1}$  above 361 K (Table 1). The experimental value is  $6.6 \text{ K}^{-1}$ , which does not agree with the values obtained from the slope of the lines.<sup>70</sup> In Figure 3, the rate of thermal expansion is also indicated as a function of each temperature range, which indicates that the calculated values correspond to the experimental ones in the range above 400 K.

For the cellulose thin film, the volumetric thermal expansion appears to be composed of two linear regions with different slopes, which is indicative of a second-order phase transition around 383 K where the two lines intersect. As given in Table 1, the coefficient of thermal expansion is  $1.5 \times 10^{-4} \text{ K}^{-1}$  at temperatures below 383 K and  $2.2 \times 10^{-4} \text{ K}^{-1}$  at temperatures above 383 K. The former value is in agreement with the range of  $0.9 - 1.4 \times 10^{-4} \text{ K}^{-1}$  reported by Vainio for temperatures below 300 K.<sup>71</sup> The molecular model of the cellulose thin film was built with 1,4- $\beta$ -D-glucose oligomers, and there was no crystal in the structure, so the transition occurred due to some order-disorder transition. The  $T_g$  of cellulose has been difficult to measure experimentally since it is estimated to exist near or above its thermal decomposition temperature. The  $T_g$  of rayon was measured to be greater than 513 K,<sup>33</sup> and for cellulose, it has been estimated from multiple computational methods to be between 243 and 650 K.<sup>61</sup> Just as mentioned above, the  $T_g$  for a thin film is expected to be 50–70 degrees lower than in the bulk. Thus, the second-order phase transition observed at 383 K could be attributed to  $T_g$ . An alternative hypothesis is that this phase transition is due to significant breakage of hydrogen bonds between cellulose chains at 383 K, which is in the temperature range of water loss (373–393 K) reported from thermal gravimetry and differential calorimetry analyses.<sup>72</sup> A similar hypothesis has also been used to explain second-order phase transitions observed in experiments with wood components.<sup>73</sup> By studying Figure 3 further, another second-order phase transition could be observed to exist in the 525–571 K temperature range, in which the thermal expansion is the lowest, but there is no cross point of the fitting lines for cellulose. This subtle

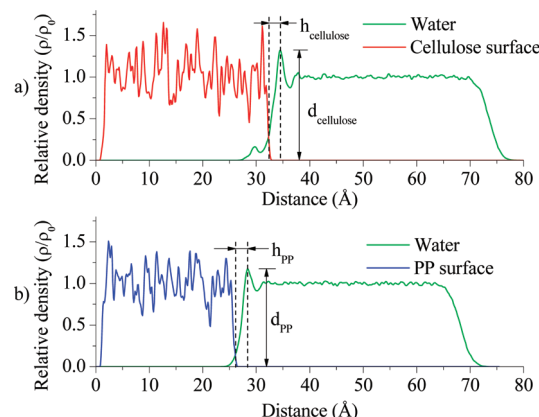


**Figure 4.** The relative density profiles of polymer–water–vacuum models for (a) cellulose and (b) PP. The relative density is calculated by  $\rho/\rho_0$ , in which  $\rho$  is the local density and  $\rho_0$  is the bulk density. The values of the quantities indicated in the figure are given in Table 3.

transition could also be attributed to the  $T_g$  of cellulose. However, this transition would be subtle if it indeed exists. As noted above, these temperatures are in the range of the thermal decomposition of cellulose; the classical MD simulations performed here do not allow thermal decomposition to occur since covalent bonds cannot be broken.

**Surface Interactions with Water.** Water was placed on top of each polymer surface, and then vacuum was added on top to allow water to just interact with one side of the layer. From this setup, the interaction energy between the polymer layer and water was calculated and compared to the free surface cohesive energy of water of  $-72.8 \text{ mJ/m}^2$ .<sup>65</sup> The interaction energy was calculated to be  $-179.5 \text{ mJ/m}^2$  for cellulose and  $-41.0 \text{ mJ/m}^2$  for PP (Table 3). Since more negative energy indicates larger attraction, interactions of water with cellulose are about 4.5 times stronger than with PP. By comparing these values to the free surface cohesive energy of water, it can be concluded that the interactions between water and cellulose are attractively stronger than those between water and PP, in line with the respective hydrophilic and hydrophobic character of cellulose and PP, respectively.

As indicated in Table 3, the interaction energy between water and PP is mostly comprised of van der Waals interactions; there is very little electrostatic energy and no hydrogen bonding because PP does not have any polar groups or H-bond donors/acceptors. On the contrary, the interaction energy with cellulose is comprised mostly of electrostatic and hydrogen bonding energies, with the latter being the most important and explained by the interactions between water and the hydroxyl groups of cellulose. The van der Waals energy makes a small contribution to the total energy with a value on the same order as that for water and PP.

To characterize the interfacial behaviors more fully, the relative density profiles along the normal direction of the surfaces are given in Figure 4. In this work, the interfacial boundary is defined as the cross-point position of the curves for water and the polymer surface. These results indicate that the relative density at the water–cellulose interface is 1.4 times higher than the bulk density, which could be mainly due to adhesion that is driven by the strong H-bond interactions with the cellulose surface, leading to more compact water molecules within the vicinity. The interface between water and PP also has a slightly higher density

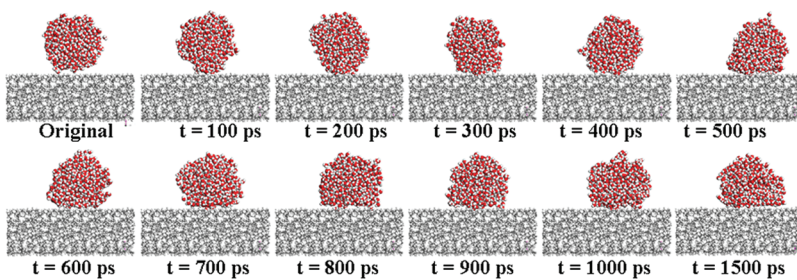


**Figure 5.** The dynamics of a water nanodroplet on the amorphous PP surface. Atom colors are indicated by red (oxygen), gray (carbon), and white (hydrogen).

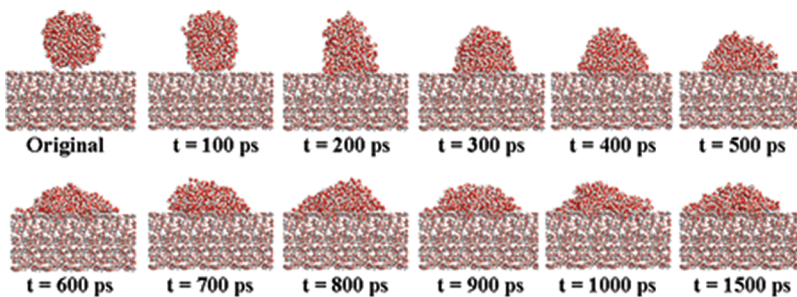


**Figure 6.** Same as Figure 5 but for the amorphous cellulose surface.

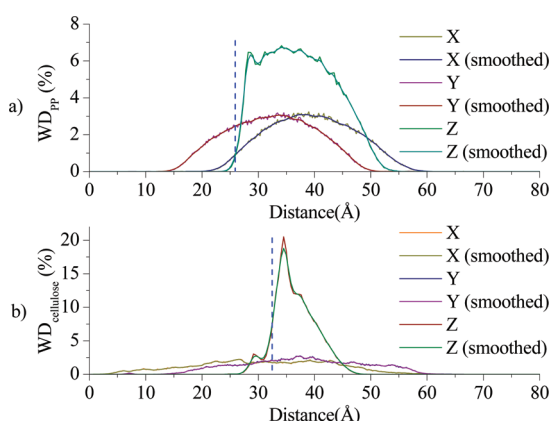


**Figure 7.** The weight distributions of water molecules on the PP and cellulose surfaces,  $WD_{cellulos}$  and  $WD_{PP}$ , in each  $X$ ,  $Y$ ,  $Z$  dimension, calculated from 1000 to 1500 ps of the MD simulation. The water droplet is on the (a) PP and (b) cellulose surfaces. The dashed lines indicate the surface position at the  $Z$  axis.

relative to the bulk, which could be due to the interplay between the fast diffusion of the water molecules and the hydrophobic nature of PP. In addition, a relatively small water density is observed on the polymer (left) side of the interfacial boundary in both cases, which is due to the minor “dents” in the surfaces (parts c and d of Figure 1) due to the molecular surface roughness. There is significantly higher water density observed in the cellulose layer compared to that of PP, which suggests that some water molecules may be permeating the cellulose surface in order to optimize the number of favorable hydrogen bond interactions.

The CA of a fluid on a solid surface is sensitive to its surface energy and can be used to quantify properties such as wettability. Figures 5 and 6 provide the evolution in the CA of a water nanodroplet on the PP and cellulose amorphous surfaces, respectively,

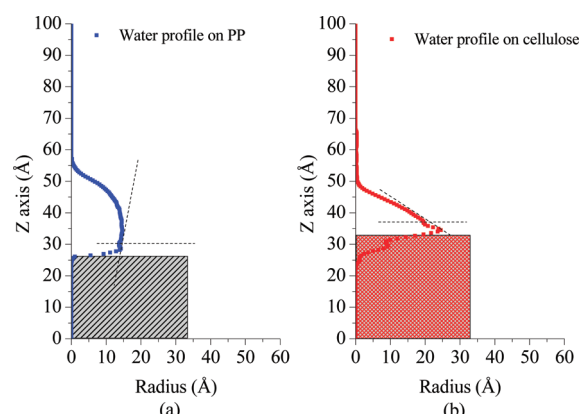


**Figure 8.** The average shapes of the water nanodroplet on the PP (a) and cellulose (b) surfaces from the time interval of 1000 to 1500 ps. The hatched boxes refer to the solid film positions of PP and cellulose, respectively. The black slash lines are the tangent line of the shape.

during the MD simulations. The water nanodroplet on a PP surface in Figure 5 reaches the system equilibrium in around  $t = 600$  ps, and the change in shape of the nanodroplet is negligible. There is no wetting on the PP surface due to its hydrophobicity. In contrast, the water nanodroplet on the cellulose surface in Figure 6 spreads out and reaches CA equilibrium by 1000 ps.

The distribution of water molecules on the PP and cellulose surfaces as a function of axis direction ( $X$ ,  $Y$ ,  $Z$ ) is given in Figure 7; the blue dashed line indicates where the thin film of PP or cellulose begins. The water nanodroplet on the PP thin film was fairly symmetric in all three directions. In the  $z$  direction, practically all of the water molecules were located to the right side of the dashed line, indicating that very few water molecules diffused into the PP amorphous surface. In contrast, the distribution of the water nanodroplet in the  $X$  and  $Y$  directions on

the cellulose thin film was asymmetric. This asymmetry can be due to two factors. First, the intermolecular space was randomly distributed in the amorphous layer and consequently, the water molecules randomly penetrated the layer in those dimensions. Second, the surface roughness impacted the spreading of the fluid on the surface. In the Z axis direction, the water molecules were distributed close to the cellulose surface boundary (dashed line) due to its hydrophilicity.

Although these distribution curves help to quantify the shape of the water in the three dimensions, it cannot directly provide the value of the CA.<sup>76–78</sup> The radius ( $r$ ) of the water droplet can be calculated from the following equation

$$\pi r^2 \Delta z \rho = \Delta m \Rightarrow r = \sqrt{\frac{1}{\rho \pi} \times \frac{\Delta m}{\Delta z}} \quad (2)$$

where  $\rho$  is the water density assumed to be 1 g/cm<sup>3</sup>, and  $\Delta m/\Delta z$  is the weight distribution along the Z axis (normal to the surface). The shape of the water nanodroplet can be drawn in terms of  $r$  and  $z$ , as given in Figure 8. To avoid the effect of the density shift of the liquid–solid interface, the points of the profiles below a height of 4.5 Å on each surfaces were used to fit the CA lines. CA angle values were determined by the tangent line, which were obtained by the slope of a pair of the shape-line points close to the surface plane (see horizontal reference lines in Figure 8). The CAs of the PP and cellulose thin films are  $106 \pm 4$  and  $33 \pm 3^\circ$ , respectively (Table 1). These calculated values are in agreement with experimental measurements of  $103$  and  $29^\circ$  for spin-coated films of PP and cellulose, respectively.<sup>74</sup> The water CA on PP from our model agrees with experimental values<sup>79</sup> and with results from recent simulations with amorphous PP.<sup>49</sup> The CAs on cellulose depend on its crystallinity, ranging from  $24$  to  $50^\circ$ .<sup>21</sup> CA simulations performed on crystalline cellulose yielded CAs on the order of  $70$ – $120^\circ$ ,<sup>50</sup> thus suggesting that amorphous cellulose is more hydrophilic than crystalline forms. This observation is likely due to the decrease in the density and the increase in molecular surface roughness, thus exposing more hydroxyl groups to the water molecules. Most importantly, the results of the CAs agree with observations from the calculated surface energy whereby the nonbond contribution is found to play a major role in the confined surface model.

## CONCLUSIONS

The use of a soft confining layer comprised of a xenon crystal in MD simulations for building amorphous layers is the key component to compact linear- or ring-chain polymers into a proper density distribution that corresponds well the actual material. The physical properties of amorphous PP and the cellulose films built with this method agree with experimental values. The suitability of the proposed polymer layers to study interactions of PP and cellulose with water was illustrated. Overall, the results of the simulations indicate the usefulness of our approach of fixing fractional positions in MD as a feasible method to create structures mimicking amorphous polymer substrates, with polymer chains compacted or not.

## AUTHOR INFORMATION

### Corresponding Author

\*E-mail: melissa\_pasquinelli@ncsu.edu. Phone: (919) 515-9426. Fax: (919) 515-6532.

## Present Addresses

<sup>†</sup>Department of Earth and Atmospheric Science, Cornell University, Ithaca, NY 14853.

## ACKNOWLEDGMENT

We acknowledge support of the National Textile Center under Grant No. C05-NS09. We also thank Dr. Juan P. Hinestroza at Cornell University for useful discussions.

## REFERENCES

- (1) Hearle, J. W. S. *Polymers and their properties*; Horwood, E., Ed.; Halsted Press: Chichester; New York, 1982.
- (2) Ellison, C. J.; Torkelson, J. M. *Nat. Mater.* **2003**, *2*, 695.
- (3) Buell, S.; Rutledge, G. C.; Vliet, K. J. V. *ACS Appl. Mater. Interfaces* **2010**, *2*, 1164.
- (4) Liu, Y.; Garcia, C. D.; Henry, C. S. *Analyst* **2003**, *128*, 1002.
- (5) Whitesides, G. M. *Nat. Biotechnol.* **2003**, *21*, 1161.
- (6) Tang, Z.; Wang, Y.; Podsiadlo, P.; Kotov, N. A. *Adv. Mater.* **2006**, *18*, 3203.
- (7) Guo, C. X.; Zheng, X. T.; Lu, Z. S.; Lou, X. W.; Li, C. M. *Adv. Mater.* **2010**, *22*, 5164.
- (8) Jeong, H. J.; Pyun, W. H.; Yang, S. Y. *Macromol. Rapid Commun.* **2009**, *30*, 1109.
- (9) Tokarev, I.; Motornov, M.; Minko, S. *J. Mater. Chem.* **2009**, *19*, 6932.
- (10) Song, J.; Liang, J.; Liu, X.; Krause, W. E.; Hinestroza, J. P.; Rojas, O. J. *Thin Solid Films* **2009**, *517*, 4348.
- (11) Brinker, C. J.; Frye, G. C.; Hurd, A. J.; Ashley, C. S. *Thin Solid Films* **1991**, *201*, 97.
- (12) Hall, D. B.; Underhill, P.; Torkelson, J. M. *Polym. Eng. Sci.* **1998**, *38*, 2039.
- (13) Wu, C. C.; Wu, C. I.; Sturm, J. C.; Kahn, A. *Appl. Phys. Lett.* **1997**, *70*, 1348.
- (14) Malinauskas, A. *Polymer* **2001**, *42*, 3957.
- (15) Lange, F. F. *Science* **1996**, *273*, 903.
- (16) Tanaka, K.; Takahara, A.; Kajiyama, T. *Macromolecules* **1996**, *29*, 3232.
- (17) Abe, Y.; Kokubo, T.; Yamamuro, T. *J. Mater. Sci.: Mater. Med.* **1990**, *1*, 233.
- (18) Flack, W. W.; Soong, D. S.; Bell, A. T.; Hess, D. W. *J. Appl. Phys.* **1984**, *56*, 1199.
- (19) Gunnars, S.; Wåberg, L.; Cohen Stuart, M. A. *Cellulose* **2002**, *9*, 239.
- (20) Stephens, C. H.; Whitmore, P. M.; Morris, H. R.; Bier, M. E. *Biomacromolecules* **2008**, *9*, 1093.
- (21) Aulin, C.; Ahok, S.; Josefsson, P.; Nishino, T.; Hirose, Y.; Österberg, M.; Wagberg, L. *Langmuir* **2009**, *25*, 7675.
- (22) Gehlen, M. H. *Cellulose* **2010**, *17*, 245.
- (23) Yu, Y.; Wu, H. *Ind. Eng. Chem. Res.* **2010**, *49*, 3902.
- (24) Kontturi, E.; Tammelin, T.; Österberg, M. *Chem. Soc. Rev.* **2006**, *35*, 1287.
- (25) Kontturi, E.; Suchy, M.; Penttilä, P.; Jean, B.; Pirkkalainen, K.; Torkkeli, M.; Serimaa, R. *Biomacromolecules* **2011**, *12*, 770.
- (26) Yan, M.; Ren, J. *J. Mater. Chem.* **2005**, *15*, 523.
- (27) Notley, S. M.; Eriksson, M.; Wåberg, L.; Beck, S.; Gray, D. G. *Langmuir* **2006**, *22*, 3154.
- (28) Li, Y.; Liu, H.; Song, J.; Rojas, O. J.; Hinestroza, J. P. *ACS Appl. Mater. Interfaces* **2011**, *3*, 2349.
- (29) Liu, X.; Song, J.; Wu, D.; Genzer, J.; Theyson, T.; Rojas, O. J. *Ind. Eng. Chem. Res.* **2010**, *49*, 8550.
- (30) Liu, X.; Vesterinen, A.-H.; Genzer, J.; Seppälä, J. V.; Rojas, O. J. *Langmuir* **2011**, *27*, 9769.
- (31) Liu, X.; Wu, D.; Turgman-Cohen, S.; Genzer, J.; Theyson, T. W.; Rojas, O. J. *Langmuir* **2010**, *26*, 9565.
- (32) Mazeau, K.; Vergelati, C. *Langmuir* **2002**, *18*, 1919.
- (33) Gill, R. A.; Steele, R. J. *Appl. Polym. Sci.* **1961**, *5*, 589.

- (34) Queyroy, S.; Neyertz, S.; Brown, D.; Müller-Plathe, F. *Macromolecules* **2004**, *37*, 7338.
- (35) Theodorou, D. N.; Suter, U. W. *Macromolecules* **1985**, *18*, 1467.
- (36) Hapke, T.; Linke, A.; Pätzold, G.; Heermann, D. W. *Surf. Sci.* **1997**, *373*, 109.
- (37) Misra, S.; Fleming, P. D.; Mattice, W. L. *J. Comput.-Aided Mater. Des.* **1995**, *2*, 101.
- (38) Natarajan, U.; Tanaka, G.; Mattice, W. L. *J. Comput.-Aided Mater. Des.* **1998**, *4*, 193.
- (39) He, D.; Reneker, D. H.; Mattice, W. L. *Comput. Theor. Polym. Sci.* **1997**, *7*, 19.
- (40) Prathab, B.; Aminabhavi, T. M.; Parthasarathi, R.; Manikandan, P.; Subramanian, V. *Polymer* **2006**, *47*, 6914.
- (41) Prathab, B.; Aminabhavi, T. M. *J. Polym. Sci., Part B: Polym. Phys.* **2007**, *45*, 1260.
- (42) Prathab, B.; Subramanian, V.; Aminabhavi, T. M. *Polymer* **2007**, *48*, 409.
- (43) Yu, X.; Wu, R.; Yang, X. *J. Phys. Chem. B* **2010**, *114*, 4955.
- (44) Clancy, T. C.; Mattice, W. L. *Comput. Theor. Polym. Sci.* **1999**, *9*, 261.
- (45) Raffaini, G.; Elli, S.; Ganazzoli, F. *J. Biomed. Mater. Res., Part A* **2006**, *77A*, 618.
- (46) Hirvi, J. T.; Pakkanen, T. A. *J. Chem. Phys.* **2006**, *125*, 144712.
- (47) Wang, Y. C.; Hsieh, J. Y.; Chen, C.; Chang, J. G.; Lin, J. S.; Ju, S. P.; Wang, H. H.; Lee, W. J. *J. Nanosci. Nanotechnol.* **2010**, *10*, 7075.
- (48) Lee, W. J.; Chang, J. G.; Ju, S. P. *Langmuir* **2010**, *26*, 12640.
- (49) Dai, Z. W.; Ling, J.; Huang, X. J.; Wan, L. S.; Xu, Z. K. *J. Phys. Chem. C* **2011**, *115*, 10702.
- (50) Mazeau, K.; Rivet, A. *Biomacromolecules* **2008**, *9*, 1352.
- (51) Accelrys; Accelrys Software Inc.: San Diego, 2001–2011.
- (52) Sun, H. *J. Phys. Chem. B* **1998**, *102*, 7338.
- (53) Liu, H. Fiber Lubrication: A Molecular Dynamics Simulation Study. Ph.D. Thesis, NC State University, 2009.
- (54) Düren, T.; Millange, F.; Férey, G.; Walton, K. S.; Snurr, R. Q. *J. Phys. Chem. C* **2007**, *111*, 15350.
- (55) Sun, C. C. *J. Pharm. Sci.* **2005**, *94*, 2061.
- (56) Michaels, A. S.; Vieth, W. R.; Alcalay, H. H. *J. Appl. Polym. Sci.* **1968**, *12*, 1621.
- (57) Spaleck, W.; Moore, E. P., Jr. *Angew. Chem.* **1997**, *36*, 534.
- (58) Chen, W.; Lickfield, G. C.; Yang, C. Q. *Polymer* **2004**, *45*, 7357.
- (59) Chen, W.; Lickfield, G. C.; Yang, C. Q. *Polymer* **2004**, *45*, 1063.
- (60) Derecskei, B.; Derecskei-Kovacs, A. *Mol. Simul.* **2006**, *32*, 109.
- (61) Mazeau, K.; Heux, L. *J. Phys. Chem. B* **2003**, *107*, 2394.
- (62) Bicerano, J. *Prediction of Polymer Properties*; Marcel Dekker: New York, 2002.
- (63) Zhao, S.; Zhang, W.; Zhang, F.; Li, B. *Polym. Bull.* **2008**, *61*, 189.
- (64) Gibbs, J. W. *Scientific papers*; Dover Publications: New York, 1961.
- (65) Mirabedini, S. M.; Rahimi, H.; Hamedifar, S.; Mohsen Mohseni, S. *Int. J. Adhesion Adhesives* **2004**, *24*, 163.
- (66) Garnier, G.; Glasser, W. G. *Polym. Eng. Sci.* **1996**, *36*, 885.
- (67) Vasile, C. *Handbook of polyolefins*; Marcel Dekker: New York, 2000.
- (68) Keddie, J. L.; Jones, R. A. L.; Cory, R. A. *EPL* **1994**, *27*, 59.
- (69) Torres, J. A.; Nealey, P. F.; de Pablo, J. J. *Phys. Rev. Lett.* **2000**, *85*, 3221.
- (70) Mark, J. E. *Physical properties of polymers handbook*; Springer: New York, 2007.
- (71) Vainio, U. Characterisation of Cellulose- and Lignin-based Materials Using X-ray Scattering Methods. Ph.D. Thesis, University of Helsinki, 2007.
- (72) Szczęśniak, L.; Rachocki, A.; Tritt-Goc, J. *Cellulose* **2008**, *15*, 445.
- (73) Ramiah, M. V.; Goring, D. A. I. *J. Polym. Sci., Part C: Polym. Symp.* **1965**, *11*, 27.
- (74) Song, J. Adsorption of Amphoteric and Nonionic Polymers on Model Thin Films. Ph.D. Thesis, NC State University, 2008.
- (75) Schonhorn, H. *J. Phys. Chem.* **1966**, *70*, 4086.
- (76) Giovambattista, N.; Debenedetti, P. G.; Rossky, P. J. *J. Phys. Chem. B* **2007**, *111*, 9581.
- (77) Lundgren, M.; Allan, N. L.; Cosgrove, T.; George, N. *Langmuir* **2002**, *18*, 10462.
- (78) Werder, T.; Walther, J. H.; Jaffe, R. L.; Halicioglu, T.; Koumoutsakos, P. *J. Phys. Chem. B* **2003**, *107*, 1345.
- (79) Schonhorn, H. *Nature* **1966**, *210*, 896.